CROSSFORMER: A VERSATILE VISION TRANSFORMER HINGING ON CROSS-SCALE ATTENTION

Anonymous authors
Paper under double-blind review

ABSTRACT

Transformers have made great progress in dealing with computer vision tasks. However, existing vision transformers do not yet possess the ability of building the interactions among features of different scales, which is perceptually important to visual inputs. The reasons are two-fold: (1) Input embeddings of each layer are equal-scale, so no cross-scale feature can be extracted; (2) to lower the computational cost, some vision transformers merge adjacent embeddings inside the self-attention module, thus sacrificing small-scale (fine-grained) features of the embeddings and also disabling the cross-scale interactions. To this end, we propose **C**ross-scale **E**mbedding **L**ayer (CEL) and **L**ong **S**hort **D**istance **A**ttention (LSDA). On the one hand, CEL blends each embedding with multiple patches of different scales, providing the self-attention module itself with cross-scale features. On the other hand, LSDA splits the self-attention module into a short-distance one and a long-distance counterpart, which not only reduces the computational burden but also keeps both small-scale and large-scale features in the embeddings. Through the above two designs, we achieve cross-scale attention. Besides, we put forward a dynamic position bias for vision transformers to make the popular relative position bias apply to variable-sized images. Hinging on the cross-scale attention module, we construct a versatile vision architecture, dubbed CrossFormer, which accommodates variable-sized inputs. Extensive experiments show that CrossFormer outperforms the other vision transformers on image classification, object detection, instance segmentation, and semantic segmentation tasks.[1]

1 INTRODUCTION

It turns out that transformer (Vaswani et al., 2017; Devlin et al., 2019; Brown et al., 2020) has achieved great success in the field of natural language processing (NLP). Benefitting from its self-attention module, transformer is born with the key ability to build long-distance dependencies. Since long-distance dependencies are also needed by a number of vision tasks (Zhang & Yang, 2021; Chu et al., 2021), a surge of research work (Dosovitskiy et al., 2021; Touvron et al., 2021; Wang et al., 2021) has been conducted to explore various transformer-based vision architectures.

A transformer requires a sequence of embeddings[2](*e.g.*, word embeddings) as input. To adapt this requirement to typical vision tasks, most existing vision transformers (Dosovitskiy et al., 2021; Touvron et al., 2021; Wang et al., 2021; Liu et al., 2021b) produce embeddings by splitting an input image into equal-sized patches. For example, a 224×224 image can be split into 56×56 patches of size 4×4, and these patches are projected through a linear layer to yield an embedding sequence. Inside a certain transformer, self-attention is engaged to build the interactions between any two embeddings. Thus, the computational or memory cost of the self-attention module is $O(N^2)$, where N is the length of an embedding sequence. Such a cost is too big for a visual input because its embedding sequence is much longer than that of NLP. Therefore, the recently proposed vision transformers (Wang et al., 2021; Liu et al., 2021b; Lin et al., 2021) develop multiple substitutes to approximate the vanilla self-attention module with a lower cost.

Though the aforementioned vision transformers have made some progress, they suffer from an issue that restricts their performance – **They fail to build the interactions among features of different scales, whereas such an ability is very vital for a lot of vision tasks**. For example, an image often

[1]The code has been submitted along with our supplementary material.

[2]In this paper, we also use "embeddings" to represent the input of each layer.

contains many objects of different scales, and to fully understand the image, building the interactions among those objects is helpful. Besides, some particular tasks such as instance segmentation need the interactions between large-scale (coarse-grained) features and small-scale (fine-grained) ones. Existing vision transformers fail to deal with the above cases due to two reasons: (1) The embeddings are generated from equal-sized patches, so they only own features of one single scale. Moreover, their scales are kept unchanged or enlarged uniformly through operations like average pooling in the following layers. Hence, embeddings in the same layer are always equal-scale. (2) Inside the self-attention module, adjacent embeddings are often grouped together and merged (Wang et al., 2021; Chu et al., 2021). Since the number of groups is smaller than that of embeddings, such behavior can reduce the computational budget of the self-attention. In this case, however, even if embeddings have both small-scale and large-scale features, merging operations will lose the small-scale (fine-grained) features of each individual embedding, thereby disabling the cross-scale attention.

To enable the building of cross-scale interactions, we co-design a novel embedding layer and self-attention module as follows. 1) *Cross-scale Embedding Layer (CEL)* – Following Wang et al. (2021), we also employ a pyramid structure for our transformer, which naturally splits the vision transformer model into multiple stages. CEL appears at the start of each stage, which receives last stage's output (or an input image) as input and samples patches with multiple kernels of different scales (*e.g.*, 4×4 or 8×8). Then, each embedding is constructed by projecting and concatenating these patches as opposed to solely using one single-scale patch, which endows each embedding with cross-scale features. 2) *Long Short Distance Attention (LSDA)* – We propose a substitute of the vanilla self-attention, but to preserve small-scale features, the embeddings will not be merged. In contrast, we split the self-attention module into *Short Distance Attention* (SDA) and *Long Distance Attention* (LDA). SDA builds the dependencies among neighboring embeddings, while LDA takes charge of the dependencies among embeddings far away from each other. The proposed LSDA can also reduce the cost of the self-attention module like previous studies (Wang et al., 2021; Chu et al., 2021), but different from them, LSDA does not undermine either small-scale or large-scale features. As a consequence, attention with cross-scale interactions is enabled.

Besides, following prior work (Shaw et al., 2018; Liu et al., 2021b), we employ a relative position bias for embeddings' position representations. The Relative Position Bias (RPB) only supports fixed image/group size[3]. However, image size for many vision tasks such as object detection is variable, so does group size for many architectures, including ours. To make the RPB more flexible, we further introduce a trainable module called *Dynamic Position Bias* (DPB), which receives two embeddings' relative distance as input and outputs their position bias. The DPB module is optimized end-to-end in the training phase, inducing an ignorable cost but making RPB apply to variable image/group size.

All our proposed modules can be implemented with about ten lines of code. Based on them, we construct four versatile vision transformers of different sizes, dubbed *CrossFormers*. Other than image classification, the proposed CrossFormer can handle a variety of tasks with variable-sized inputs such as object detection. Experiments on four representative vision tasks (*i.e.*, image classification, object detection, instance segmentation, and semantic segmentation) demonstrate that CrossFormer outperforms the other state-of-the-art vision transformers on all the tasks. Remarkably, the performance gains brought by CrossFormer are substantially significant on dense prediction tasks, *e.g.*, object detection and instance/semantic segmentation.

It is worth highlighting our contributions as follows:

- We propose cross-scale embedding layer (CEL) and long short distance attention (LSDA), which together compensate for existing transformers' incapability of building cross-scale attention.
- The dynamic position bias module (DPB) is further proposed to make the relative position bias more flexible, *i.e.*, accommodating variable image size or group size.
- Multiple CrossFormers with different sizes are constructed, and we corroborate their effectiveness through sufficient experiments on four representative vision tasks.

2 BACKGROUND

Vision Transformers. Motivated by the transformers developed for NLP, researchers design specific visual transformers for vision tasks to take full advantage of their powerful attention mechanism. In

[3]Some vision transformers split input embeddings into several groups. Group size means the number of embeddings in a group.

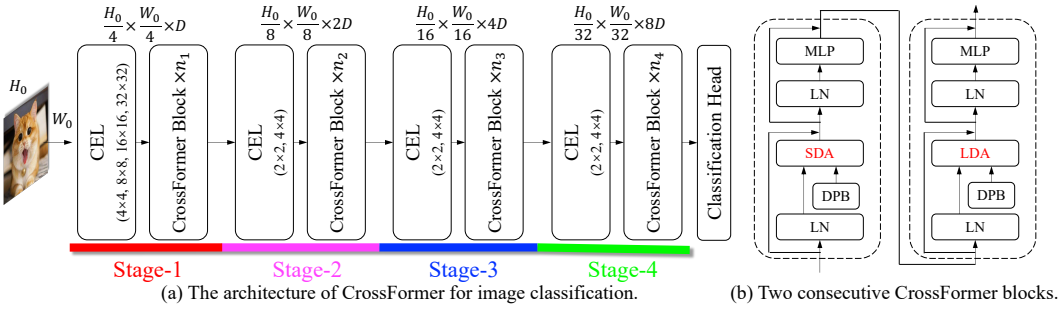

(a) The architecture of CrossFormer for image classification. (b) Two consecutive CrossFormer blocks.

Figure 1: (a) The architecture of CrossFormer for classification. The input size is $H_0 \times W_0$, and the size of feature maps in each stage is shown on the top. *Stage-i* consists of a CEL and n_i CrossFormer blocks. Numbers in CELs represent kernels' sizes used for sampling patches. (b) The inner structure of two consecutive CrossFormer blocks. SDA and LDA appear alternately in different blocks.

particular, ViT and DeiT transfer the original transformer Vaswani et al. (2017) to vision tasks (Touvron et al., 2021; Dosovitskiy et al., 2021), achieving impressive performance. Later, PVT (Wang et al., 2021), HVT (Pan et al., 2021), Swin (Liu et al., 2021b), and ViTAE (Xu et al., 2021) introduce a pyramid structure into the visual transformers, greatly decreasing the number of patches in the later layers of a respective model. They also extend the visual transformers to other vision tasks like object detection and segmentation (Wang et al., 2021; Liu et al., 2021b).

Substitutes of Self-attention. As the core component of transformers, the self-attention module incurs the $O(N^2)$ computational/memory cost, where N is the length of an embedding sequence. Though such a cost may be acceptable for image classification, it is not the case for other tasks with much larger input images (*e.g.*, object detection and segmentation). To alleviate the cost, Swin (Liu et al., 2021b) restricts the attention in a certain local region, giving up long-distance dependencies. PVT (Wang et al., 2021) and Twins (Chu et al., 2021) make adjacent embeddings share the same *key/value* to reduce the cost. Likewise, other vision transformers such as (Chen et al., 2021a; Zhang et al., 2021b; Wu et al., 2021) also employ a divide-and-conquer method and approximate the vanilla self-attention module with a lower cost.

Position Representations. Transformer is combination-invariant. That is, shuffling input embeddings does not change the output of a transformer. Nevertheless, the position of embeddings also contains important information. To make the respective model aware of this, many different position representations of embeddings (Vaswani et al., 2017) are proposed. For example, Dosovitskiy et al. (2021) directly add the embeddings with the vectors that contain absolute position information. In contrast, Relative Position Bias (RPB) (Shaw et al., 2018) resorts to position information indicating the relative distance of two embeddings. Much recent work (Liu et al., 2021b; Chen et al., 2021b) shows that RPB performs better than other position representations. Motivated by this finding, our proposed position representation DPB also uses relative distance, but different from RPB that only handles fixed-sized images, our DPB applies to images with dynamic sizes.

3 CROSSFORMER

The overall architecture of CrossFormer is plotted in Figure 1. Following (Wang et al., 2021; Liu et al., 2021b; Lin et al., 2021), CrossFormer also employs a pyramid structure, which naturally splits the transformer model into four stages. Each stage consists of a cross-scale embedding layer (CEL, Section 3.1) and several CrossFormer blocks (Section 3.2). A CEL receives last stage's output (or an input image) as input and generates cross-scale embeddings. In this process, CEL (except that in *Stage-1*) reduces the number of embeddings to a quarter while doubles their dimensions for a pyramid structure. Then, several CrossFormer blocks, each of which involves long short distance attention (LSDA) and dynamic position bias (DPB), are set up after CEL. A specialized head (*e.g.*, the classification head in Figure 1) follows after the final stage accounting for a specific task.

3.1 CROSS-SCALE EMBEDDING LAYER (CEL)

Cross-scale embedding layer (CEL) is leveraged to generate input embeddings for each stage. Figure 2 takes the first CEL, which is ahead of *Stage-1*, as an example. It receives an image as input, then sampling patches using four kernels of different sizes. The stride of four kernels is kept the same

so that they generate the same number of embeddings[4]. As we can observe in Figure 2, every four corresponding patches have the same center but different scales, and all these four patches will be projected and concatenated as one embedding. In practice, the process of sampling and projecting can be fulfilled through four convolutional layers.

For a cross-scale embedding, one problem is how to set the projected dimension of each scale. The computational budget of a convolutional layer is proportional to K^2D^2, where K and D represent kernel size and input/output dimension, respectively (assuming the input dimension equals to the output dimension). Therefore, given the same dimension, a large kernel consumes more budget than a smaller one. To control the total budget of the CEL, we use a lower dimension for large kernels while a higher dimension for small kernels. Figure 2 provides the specific allocation rule in its subtable, and a 128 dimensional example is given. Compared with allocating the dimension equally, our scheme saves much computational cost but does not explicitly affect the model's performance. The cross-scale embedding layers in other stages work in a similar way. As shown in Figure 1, CELs for *Stage-2/3/4* use two different kernels (2×2 and 4×4). Further, to form a pyramid structure, the strides of CELs for *Stage-2/3/4* are set as 2×2 to reduce the number of embeddings to a quarter.

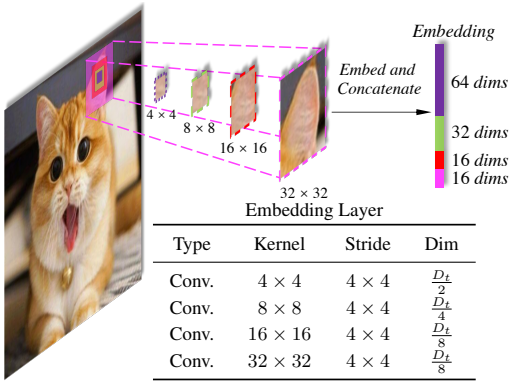

Type	Kernel	Stride	Dim
Conv.	4×4	4×4	$\frac{D_t}{2}$
Conv.	8×8	4×4	$\frac{D_t}{4}$
Conv.	16×16	4×4	$\frac{D_t}{8}$
Conv.	32×32	4×4	$\frac{D_t}{8}$

Figure 2: Illustration of the CEL layer. The input image is sampled by four different kernels (*i.e.*, $4 \times 4, 8 \times 8, 16 \times 16, 32 \times 32$) with same stride 4×4. Each embedding is constructed by projecting and concatenating the four patches. D_t means the total dimension of the embedding.

3.2 CrossFormer Block

Each CrossFormer block consists of a long short distance attention module (*i.e.*, LSDA, which involves a short distance attention (SDA) module or a long distance attention (LDA) module) and a multilayer perceptron (MLP). As shown in Figure 1b, SDA and LDA appear alternately in different blocks, and the dynamic position bias (DPB) module works in both SDA and LDA for obtaining embeddings' position representations. Following the prior vision transformers, residual connections are used in each block.

3.2.1 Long Short Distance Attention (LSDA)

We split the self-attention module into two parts: short distance attention (SDA) and long distance attention (LDA). For SDA, every $G \times G$ adjacent embeddings are grouped together. Figure 3a gives an example where $G = 3$. For LDA with input of size $S \times S$, the embeddings are sampled with a fixed interval I. For example in Figure 3b ($I = 3$), all embeddings with a red border belong to a group, and those with a yellow border comprise another group. The group's height or width for LDA is computed as $G = S/I$ (*i.e.*, $G = 3$ in this example). After grouping embeddings, both SDA and LDA employ the vanilla self-attention within each group. As a result, the memory/computational cost of the self-attention module is reduced from $O(S^4)$ to $O(S^2G^2)$, and $G \ll S$ in most cases.

It is worth noting that the effectiveness of LDA also benefits from cross-scale embeddings. Specifically, we draw all the patches comprising two embeddings in Figure 3b. As we can see, the small-scale patches of two embeddings are non-adjacent, so it is difficult to judge their relationship without the help of the context. In other words, it will be hard to build the dependency between these two embeddings if they are only constructed by small-scale patches (*i.e.*, single-scale feature). On the contrary, adjacent large-scale patches provide sufficient context to link these two embeddings, which makes long-distance cross-scale attention easier and more meaningful.

We provide the pseudo-code of LSDA in the appendix (A.1). Based on the vanilla multi-head self-attention, LSDA can be implemented with only ten lines of code. Further, only *reshape* and *permute* operations are used, so no extra computational cost is introduced.

[4]The image will be padded if necessary.

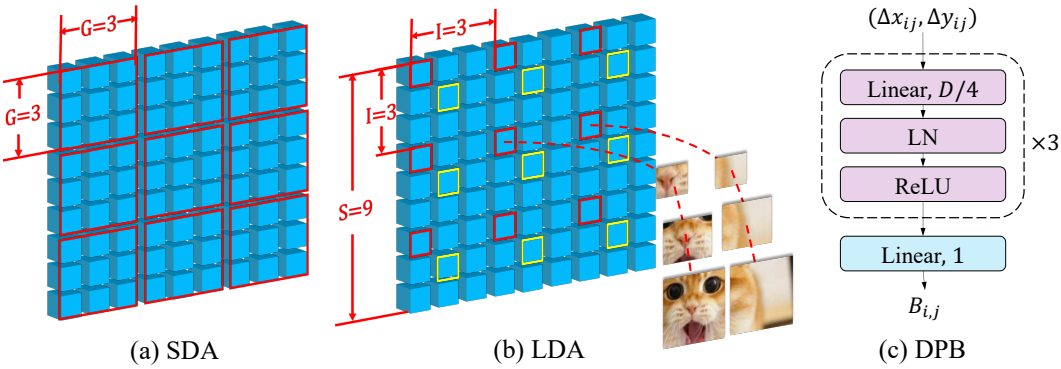

Figure 3: (a) Short distance attention (SDA). Embeddings (blue cubes) are grouped by red boxes. (b) Long distance attention (LDA). Embeddings with the same color borders belong to the same group. Large patches of embeddings in the same group are adjacent. (c) Dynamic position bias (DBP). The dimensions of intermediate layers are $D/4$, and the output is a scalar.

3.2.2 Dynamic Position Bias (DPB)

Relative position bias (RPB) indicates embeddings' relative position by adding a bias to their attention. Formally, the LSDA's attention map with RPB becomes:

$$\texttt{Attention} = \texttt{Softmax}(\boldsymbol{Q}\boldsymbol{K}^T/\sqrt{d} + \boldsymbol{B})\boldsymbol{V}, \tag{1}$$

where $\boldsymbol{Q}, \boldsymbol{K}, \boldsymbol{V} \in \mathbb{R}^{G^2 \times D}$ represent *query, key, value* in the self-attention module, respectively. $\sqrt{d}$ is a constant normalizer, and $\boldsymbol{B} \in \mathbb{R}^{G^2 \times G^2}$ is the RPB matrix. In previous works (Liu et al., 2021b), $\boldsymbol{B}_{i,j} = \hat{\boldsymbol{B}}_{\Delta x_{ij}, \Delta y_{ij}}$, where $\hat{\boldsymbol{B}}$ is a fixed-sized matrix, and $(\Delta x_{ij}, \Delta y_{ij})$ is the coordinate distance between the i_{th} and j_{th} embeddings. It is obvious that the image/group size is restricted in case that $(\Delta x_{ij}, \Delta y_{ij})$ exceeds the size of $\hat{B}$. In contrast, we propose an MLP-based module called DPB to generate the relative position bias dynamically, *i.e.*,

$$\boldsymbol{B}_{i,j} = DPB(\Delta x_{ij}, \Delta y_{ij}). \tag{2}$$

The structure of DPB is displayed in Figure 3c. Its non-linear transformation consists of three fully-connected layers with layer normalization (Ba et al., 2016) and ReLU (Nair & Hinton, 2010). The input dimension of DPB is 2, *i.e.*, $(\Delta x_{ij}, \Delta y_{ij})$, and intermediate layers' dimension is set as $D/4$, where D is the dimension of embeddings. The output B_{ij} is a scalar, encoding the relative position feature between the i_{th} and j_{th} embeddings. DPB is a trainable module optimized along with the whole transformer model. It can deal with any image/group size without worrying about the bound of $(\Delta x_{ij}, \Delta y_{ij})$. In the appendix (A.2), we prove that DPB is equivalent to RPB if the image/group size is fixed. In this case, we can transform a trained DPB to RPB in the test phase. We also provide an efficient $O(G^2)$ implementation of DPB when image/group size is variable (the complexity is $O(G^4)$ in a normal case because $\boldsymbol{B} \in \mathbb{R}^{G^2 \times G^2}$).

3.3 Variants of CrossFormer

Table 1 lists the detailed configurations of CrossFormer's four variants (-T, -S, -B, and -L for tiny, small, base, and large, respectively) for image classification. To re-use the pre-trained weights, the models for other tasks (*e.g.*, object detection) employ the same backbones as classification except that they may use different G and I. Specifically, besides the configurations same to classification, we also test with $G_1 = G_2 = 14, I_1 = 16$, and $I_2 = 8$ for the detection (and segmentation) models' first two stages to adapt to larger images. The specific configurations are described in the appendix (A.3). Notably, the group size or the interval (*i.e.*, G or I) does not affect the shape of weight tensors, so the backbones pre-trained on ImageNet can be readily fine-tuned on other tasks even though they use different G or I.

4 Experiments

The experiments are carried out on four challenging tasks: image classification, object detection, instance segmentation, and semantic segmentation. To entail a fair comparison, we keep the same data

Table 1: Variants of CrossFormer for image classification. The example input size is 224×224. S represents the feature maps' height (and width) of each stage. D and H mean embedding dimensions and the number of heads in the multi-head self-attention module, respectively. G and I are group size and interval for SDA and LDA, respectively.

	Output Size	Layer Name	CrossFormer-T	CrossFormer-S	CrossFormer-B	CrossFormer-L
Stage-1	56×56 $(S_1 = 56)$	Cross Embed.	Kernel size: 4×4, 8×8, 16×16, 32×32, Stride=4			
		SDA/LDA MLP	$\begin{bmatrix} D_1 = 64 \\ H_1 = 2 \\ G_1 = 7 \\ I_1 = 8 \end{bmatrix} \times 1$	$\begin{bmatrix} D_1 = 96 \\ H_1 = 3 \\ G_1 = 7 \\ I_1 = 8 \end{bmatrix} \times 2$	$\begin{bmatrix} D_1 = 96 \\ H_1 = 3 \\ G_1 = 7 \\ I_1 = 8, \end{bmatrix} \times 2$	$\begin{bmatrix} D_1 = 128 \\ H_1 = 4 \\ G_1 = 7 \\ I_1 = 8 \end{bmatrix} \times 2$
Stage-2	28×28 $(S_2 = 28)$	Cross Embed.	Kernel size: 2×2, 4×4, Stride=2			
		SDA/LDA MLP	$\begin{bmatrix} D_2 = 128 \\ H_2 = 4 \\ G_2 = 7 \\ I_2 = 4 \end{bmatrix} \times 1$	$\begin{bmatrix} D_2 = 192 \\ H_2 = 6 \\ G_2 = 7 \\ I_2 = 4 \end{bmatrix} \times 2$	$\begin{bmatrix} D_2 = 192 \\ H_2 = 6 \\ G_2 = 7 \\ I_2 = 4 \end{bmatrix} \times 2$	$\begin{bmatrix} D_2 = 256 \\ H_2 = 8 \\ G_2 = 7 \\ I_2 = 4 \end{bmatrix} \times 2$
Stage-3	14×14 $(S_3 = 14)$	Cross Embed.	Kernel size: 2×2, 4×4, Stride=2			
		SDA/LDA MLP	$\begin{bmatrix} D_3 = 256 \\ H_3 = 8 \\ G_3 = 7 \\ I_3 = 2 \end{bmatrix} \times 8$	$\begin{bmatrix} D_3 = 384 \\ H_3 = 12 \\ G_3 = 7 \\ I_3 = 2 \end{bmatrix} \times 6$	$\begin{bmatrix} D_3 = 384 \\ H_3 = 12 \\ G_3 = 7 \\ I_3 = 2 \end{bmatrix} \times 18$	$\begin{bmatrix} D_3 = 512 \\ H_3 = 16 \\ G_3 = 7 \\ I_3 = 2 \end{bmatrix} \times 18$
Stage-4	7×7 $(S_4 = 7)$	Cross Embed.	Kernel size: 2×2, 4×4, Stride=2			
		SDA/LDA MLP	$\begin{bmatrix} D_4 = 512 \\ H_4 = 16 \\ G_4 = 7 \\ I_4 = 1 \end{bmatrix} \times 6$	$\begin{bmatrix} D_4 = 768 \\ H_4 = 24 \\ G_4 = 7 \\ I_4 = 1 \end{bmatrix} \times 2$	$\begin{bmatrix} D_4 = 768 \\ H_4 = 24 \\ G_4 = 7 \\ I_4 = 1 \end{bmatrix} \times 2$	$\begin{bmatrix} D_4 = 1024 \\ H_4 = 32 \\ G_4 = 7 \\ I_4 = 1 \end{bmatrix} \times 2$
Head	1×1	Avg Pooling	Kernel size: 7×7			
		Linear	Classes: 1000			

augmentation and training settings as the other vision transformers as far as possible. The competitors are all competitive vision transformers, including DeiT (Touvron et al., 2021), PVT (Wang et al., 2021), T2T-ViT (Yuan et al., 2021), TNT (Han et al., 2021), CViT (Chen et al., 2021a), Twins (Chu et al., 2021), Swin (Liu et al., 2021b), NesT (Zhang et al., 2021b), CvT (Wu et al., 2021), ViL (Zhang et al., 2021a), CAT (Lin et al., 2021), ResT (Zhang & Yang, 2021), TransCNN (Liu et al., 2021a), Shuffle (Huang et al., 2021), BoTNet (Srinivas et al., 2021), and RegionViT (Chen et al., 2021b).

4.1 Image Classification

Experimental Settings. The experiments on image classification are done with the ImageNet (Russakovsky et al., 2015) dataset. The models are trained on 1.28M training images and tested on 50K validation images. The same training settings as the other vision transformers are adopted. In particular, we use an AdamW (Kingma & Ba, 2015) optimizer training for 300 epochs with a cosine decay learning rate scheduler, and 20 epochs of linear warm-up are used. The batch size is 1,024 split on 8 V100 GPUs. An initial learning rate of 0.001 and a weight decay of 0.05 are used. Besides, we use drop path rate of $0.1, 0.2, 0.3, 0.5$ for CrossFormer-T, CrossFormer-S, CrossFormer-B, CrossFormer-L, respectively. Further, Similar to Swin (Liu et al., 2021b), RandAugment (Cubuk et al., 2020), Mixup (Zhang et al., 2018), Cutmix (Yun et al., 2019), random erasing (Zhong et al., 2020), and stochastic depth (Huang et al., 2016) are used for data augmentation.

Results. The results are shown in Table 2. As we can see, CrossFormer achieves the highest accuracy with parameters and FLOPs comparable to other state-of-the-art vision transformer structures. In specific, compared against strong baselines DeiT, PVT, and Swin, our CrossFormer outperforms them at least absolute 1.2% in accuracy on small models. Further, though RegionViT achieves the same accuracy (82.5%) as ours on a small model, it is 0.7% (84.0% vs. 83.3%) absolutely lower than ours on the large model.

4.2 Object Detection and Instance Segmentation

Experimental Settings. The experiments on object detection and instance segmentation are both done on the COCO 2017 dataset (Lin et al., 2014), which contains 118K training and 5K val images. We use MMDetection-based (Chen et al., 2019) RetinaNet (Lin et al., 2020) and Mask R-CNN (He et al., 2017) as the object detection and instance segmentation head, respectively. For both tasks,

Table 2: Results on the ImageNet validation set. The input size is 224×224 for most models, while is 384×384 for the model with a †. Results of other architectures are drawn from original papers.

Architectures	#Params	FLOPs	Acc.
PVT-S	24.5M	3.8G	79.8%
RegionViT-T	13.8M	2.4G	80.4%
Twins-SVT-S	24.0M	2.8G	81.3%
CrossFormer-T	27.8M	2.9G	**81.5%**
DeiT-S	22.1M	4.6G	79.8%
T2T-ViT	21.5M	5.2G	80.7%
CViT-S	26.7M	5.6G	81.0%
PVT-M	44.2M	6.7G	81.2%
TNT-S	23.8M	5.2G	81.3%
Swin-T	29.0M	4.5G	81.3%
NesT-T	17.0M	5.8G	81.5%
CvT-13	20.0M	4.5G	81.6%
ResT	30.2M	4.3G	81.6%
CAT-S	37.0M	5.9G	81.8%
ViL-S	24.6M	4.9G	81.8%
RegionViT-S	30.6M	5.3G	**82.5%**
CrossFormer-S	30.7M	4.9G	**82.5%**

Architectures	#Params	FLOPs	Acc.
BoTNet-S1-59	33.5M	7.3G	81.7%
PVT-L	61.4M	9.8G	81.7%
CvT-21	32.0M	7.1G	82.5%
CAT-B	52.0M	8.9G	82.8%
Swin-S	50.0M	8.7G	83.0%
RegionViT-M	41.2M	7.4G	83.1%
Twins-SVT-B	56.0M	8.3G	83.1%
NesT-S	38.0M	10.4G	83.3%
CrossFormer-B	52.0M	9.2G	**83.4%**
DeiT-B	86.0M	17.5G	81.8%
DeiT-B†	86.0M	55.4G	83.1%
ViL-B	55.7M	13.4G	83.2%
RegionViT-B	72.0M	13.3G	83.3%
Twins-SVT-L	99.2M	14.8G	83.3%
Swin-B	88.0M	15.4G	83.3%
NesT-B	68.0M	17.9G	83.8%
CrossFormer-L	92.0M	16.1G	**84.0%**

Table 3: Object detection results on COCO 2017 *val* set with RetinaNets as detectors. Results for Swin are drawn from Twins as Swin does not report results on RetinaNet. Results in blue fonts are the second-placed ones. CrossFormers with ‡ use different group sizes from classification models. (More details are put in the appendix (A.3))

Method	Backbone	#Params	FLOPs	AP^b	AP^b_{50}	AP^b_{75}	AP^b_S	AP^b_M	AP^b_L
RetinaNet 1× schedule	ResNet-50	37.7M	234.0G	36.3	55.3	38.6	19.3	40.0	48.8
	CAT-B	62.0M	337.0G	41.4	62.9	43.8	24.9	44.6	55.2
	Swin-T	38.5M	245.0G	41.5	62.1	44.2	25.1	44.9	55.5
	PVT-M	53.9M	–	41.9	63.1	44.3	25.0	44.9	57.6
	ViL-M	50.8M	338.9G	42.9	64.0	45.4	27.0	46.1	57.2
	RegionViT-B	83.4M	308.9G	43.3	65.2	46.4	29.2	46.4	57.0
	TransCNN-B	36.5M	–	43.4	64.2	46.5	27.0	47.4	56.7
	CrossFormer-S	40.8M	282.0G	**44.4** (+1.0)	65.8	47.4	28.2	48.4	59.4
	CrossFormer-S‡	40.8M	272.1G	**44.2** (+0.8)	65.7	47.2	28.0	48.0	59.1
	ResNet101	56.7M	315.0G	38.5	57.8	41.2	21.4	42.6	51.1
	PVT-L	71.1M	345.0G	42.6	63.7	45.4	25.8	46.0	58.4
	Twins-SVT-B	67.0M	322.0G	44.4	66.7	48.1	28.5	48.9	60.6
	RegionViT-B+	84.5M	328.2G	44.6	66.4	47.6	29.6	47.6	59.0
	Swin-B	98.4M	477.0G	44.7	65.9	49.2	–	–	–
	Twins-SVT-L	110.9M	455.0G	44.8	66.1	48.1	28.4	48.3	60.1
	CrossFormer-B	62.1M	389.0G	**46.2** (+1.4)	67.8	49.5	30.1	49.9	61.8
	CrossFormer-B‡	62.1M	379.1G	**46.1** (+1.3)	67.7	49.0	29.5	49.9	61.5

the backbones are initialized with the weights pre-trained on ImageNet. Then the whole models are trained with batch size 16 on 8 V100 GPUs, and an AdamW optimizer with an initial learning rate of 1×10^{-4} is used. Following previous works, we adopt $1\times$ training schedule (*i.e.*, the models are trained for 12 epochs) when taking RetinaNets as detectors, and images are resized to 800 pixels for the short side. While for Mask R-CNN, both $1\times$ and $3\times$ training schedules are used. It is noted that multi-scale training (Carion et al., 2020) is also employed when taking $3\times$ training schedules.

Results. The results on RetinaNet and Mask R-CNN are shown in Table 3 and Table 4, respectively. As we can see, the second-placed architecture changes along with the experiment, that is, these architectures may perform well on one task but poorly on another task. In contrast, our CrossFormer outperforms all the others on both tasks (detection and segmentation) with both model sizes (small and base). Further, CrossFormer's performance gain over the other architectures gets sharper when enlarging the model, indicating that CrossFormer enjoys greater potentials.

4.3 Semantic Segmentation

Experimental Settings. ADE20K (Zhou et al., 2017) is used as the benchmark for semantic segmentation. It covers a broad range of 150 semantic categories, including 20K images for training

Table 4: Object detection and instance segmentation results on COCO *val* 2017 with Mask R-CNNs as detectors. AP^b and AP^m are box average precision and mask average precision, respectively.

Method	Backbone	#Params	FLOPs	AP^b	AP^b_{50}	AP^b_{75}	AP^m	AP^m_{50}	AP^m_{75}
Mask R-CNN 1× schedule	PVT-M	63.9M	–	42.0	64.4	45.6	39.0	61.6	42.0
	Swin-T	47.8M	264.0G	42.2	64.6	46.2	39.1	61.6	42.0
	Twins-PCPVT-S	44.3M	245.0G	42.9	65.8	47.1	40.0	62.7	42.9
	TransCNN-B	46.4M	–	44.0	66.4	48.5	40.2	63.3	43.2
	ViL-M	60.1M	261.1G	43.3	65.9	47.0	39.7	62.8	42.0
	RegionViT-B	92.2M	287.9G	43.5	66.7	47.4	40.1	63.4	43.0
	RegionViT-B+	93.2M	307.1G	44.5	67.6	48.7	41.0	64.4	43.9
	CrossFormer-S	50.2M	301.0G	**45.4** (+0.9)	68.0	49.7	**41.4** (+0.4)	64.8	44.6
	CrossFormer-S‡	50.2M	291.1G	**45.0** (+0.5)	67.9	49.1	**41.2** (+0.2)	64.6	44.3
	CAT-B	71.0M	356.0G	41.8	65.4	45.2	38.7	62.3	41.4
	PVT-L	81.0M	364.0G	42.9	65.0	46.6	39.5	61.9	42.5
	Twins-SVT-B	76.3M	340.0G	45.1	67.0	49.4	41.1	64.1	44.4
	ViL-B	76.1M	365.1G	45.1	67.2	49.3	41.0	64.3	44.2
	Twins-SVT-L	119.7M	474.0G	45.2	67.5	49.4	41.2	64.5	44.5
	Swin-S	69.1M	354.0G	44.8	66.6	48.9	40.9	63.4	44.2
	Swin-B	107.2M	496.0G	45.5	–	–	41.3	–	–
	CrossFormer-B	71.5M	407.9G	**47.2** (+1.7)	69.9	51.8	**42.7** (+1.4)	66.6	46.2
	CrossFormer-B‡	71.5M	398.1G	**47.1** (+1.6)	69.9	52.0	**42.7** (+1.4)	66.5	46.1
Mask R-CNN 3× schedule	PVT-M	63.9M	–	44.2	66.0	48.2	45.0	63.1	43.5
	ViL-M	60.1M	261.1G	44.6	66.3	48.5	40.7	63.8	43.7
	Swin-T	47.8M	264.0G	46.0	68.2	50.2	41.6	65.1	44.8
	Shuffle-T	48.0M	268.0G	46.8	68.9	51.5	42.3	66.0	45.6
	CrossFormer-S‡	50.2M	291.1G	**48.7** (+1.9)	70.7	53.7	**43.9** (+1.6)	67.9	47.3
	PVT-L	81.0M	364.0G	44.5	66.0	48.3	40.7	63.4	43.7
	ViL-B	76.1M	365.1G	45.7	67.2	49.9	41.3	64.4	44.5
	Shuffle-S	69.0M	359.0G	48.4	70.1	53.5	43.3	67.3	46.7
	Swin-S	69.1M	354.0G	48.5	70.2	53.5	43.3	67.3	46.6
	CrossFormer-B‡	71.5M	398.1G	**49.8** (+1.3)	71.6	54.9	**44.5** (+1.2)	68.8	47.9

Table 5: Semantic segmentation results on the ADE20K validation set. "MS IOU" means testing with variable input size.

Semantic FPN (80K iterations)			
Backbone	#Params	FLOPs	IOU
PVT-M	48.0M	219.0G	41.6
Twins-SVT-B	60.4M	261.0G	45.0
Swin-S	53.2M	274.0G	45.2
CrossFormer-S	34.3M	220.7G	**46.0** (+0.8)
CrossFormer-S‡	34.3M	209.8G	**46.4** (+1.2)
PVT-L	65.1M	283.0G	42.1
CAT-B	55.0M	276.0G	43.6
CrossFormer-B	55.6M	331.0G	**47.7** (+4.1)
CrossFormer-B‡	55.6M	320.1G	**48.0** (+4.4)
Twins-SVT-L	103.7M	397.0G	45.8
CrossFormer-L	95.4M	497.0G	**48.7** (+2.9)
CrossFormer-L‡	95.4M	482.7G	**49.1** (+3.3)

UPerNet (160K iterations)				
Backbone	#Params	FLOPs	IOU	MS IOU
Swin-T	60.0M	945.0G	44.5	45.8
Shuffle-T	60.0M	949.0G	46.6	47.6
CrossFormer-S	62.3M	979.5G	**47.6** (+1.0)	**48.4**
CrossFormer-S‡	62.3M	968.5G	**47.4** (+0.8)	**48.2**
Swin-S	81.0M	1038.0G	47.6	49.5
Shuffle-S	81.0M	1044.0G	48.4	49.6
CrossFormer-B	83.6M	1089.7G	**49.7** (+1.3)	**50.6**
CrossFormer-B‡	83.6M	1078.8G	**49.2** (+0.8)	**50.1**
Swin-B	121.0M	1088.0G	48.1	49.7
Shuffle-B	121.0M	1096.0G	49.0	–
CrossFormer-L	125.5M	1257.8G	**50.4** (+1.4)	**51.4**
CrossFormer-L‡	125.5M	1243.5G	**50.5** (+1.5)	**51.4**

and 2K for validation. Similar to models for detection, we initialize the backbones with weights pre-trained on ImageNet, and MMSegmentation-based (Contributors, 2020) semantic FPN and UPerNet (Xiao et al., 2018) are taken as the segmentation head. For FPN (Kirillov et al., 2019), we use an AdamW optimizer with learning rate and weight deacy of 1×10^{-4}. Models are trained for 80K iterations with batch size 16. For UPerNet, an AdamW optimizer with an initial learning rate of 6×10^{-5} and a weight decay of 0.01 is used, and models are trained for 160K iterations.

Results. All results are shown in Table 5. Similar to object detection, CrossFormer exhibits a greater performance gain over the others when enlarging the model. For example, CrossFormer-T achieves 1.4% absolutely higher on IOU than Twins-SVT-B, but CrossFormer-B achieves 3.1% absolutely higher on IOU than Twins-SVT-L. Totally, CrossFormer shows a more significant advantage over the others on dense prediction tasks (*e.g.*, detection and segmentation) than on classification, implying that cross-scale interactions in the attention module are more important for dense prediction tasks than for classification.

Table 6: Results on the ImageNet validation set. The baseline model is CrossFormer-S (82.5%). We test with different kernel sizes of CELs.

CEL's Kernel Size				#Params	FLOPs	Acc.
Stage-1	*Stage-2*	*Stage-3*	*Stage-4*			
4×4	2×2	2×2	2×2	28.3M	4.5G	81.5%
8×8	2×2	2×2	2×2	28.3M	4.5G	81.9%
$4 \times 4, 8 \times 8$	$2 \times 2, 4 \times 4$	$2 \times 2, 4 \times 4$	$2 \times 2, 4 \times 4$	30.6M	4.8G	82.3%
$4 \times 4, 8 \times 8, 16 \times 16, 32 \times 32$	$2 \times 2, 4 \times 4$	$2 \times 2, 4 \times 4$	$2 \times 2, 4 \times 4$	30.7M	4.9G	**82.5%**
$4 \times 4, 8 \times 8, 16 \times 16, 32 \times 32$	$2 \times 2, 4 \times 4, 8 \times 8$	$2 \times 2, 4 \times 4$	2×2	29.4M	5.0G	82.4%

Table 7: Experimental results of ablation studies.

(a) Ablation studies on cross-scale embeddings (CEL) and long short distance attention (LSDA). The base model is CrossFormer-S (82.5%).

PVT-like	Swin-like	LSDA	CEL	Acc.
✓			✓	**81.3%**
	✓		✓	**81.9%**
		✓	✓	**82.5%**
		✓		**81.5%**

(b) Comparisons between different position representations. The base model is CrossFormer-S. Throughput is tested on $1\times$ V100 GPU.

Method	#Params/FLOPs	Throughput	Acc.
APE	30.9342M/4.9061G	686 imgs/sec	82.1%
RPB	30.6159M/4.9062G	684 imgs/sec	**82.5%**
DPB	30.6573M/4.9098G	672 imgs/sec	**82.5%**
DPB-residual	30.6573M/4.9098G	672 imgs/sec	82.4%

4.4 Ablation Studies

Cross-scale Embeddings vs. Single-scale Embeddings. We conduct the experiments by replacing cross-scale embedding layers with single-scale ones. As we can see in Table 6, when using single-scale embeddings, the 8×8 kernel in *Stage-1* brings 0.4% (81.9% vs. 81.5%) absolute improvement compared with the 4×4 kernel. It tells us that overlapping receptive fields help improve the model's performance. Besides, all models with cross-scale embeddings perform better than those with single-scale embeddings. In particular, our CrossFormer achieves 1% (82.5% vs. 81.5%) absolute performance gain compared with using single-scale embeddings for all stages. For cross-scale embeddings, we also try several different combinations of kernel sizes, and they all show similar performance ($82.3\% \sim 82.5\%$). In summary, cross-scale embeddings can bring a large performance gain, yet the model is relatively robust to different choices of kernel size.

LSDA vs. Other Self-attentions. Two self-attention modules used in PVT and Swin are compared. Specifically, PVT sacrifices the small-scale features when computing the self-attention, while Swin restricts the self-attention in a local region, giving up the long-distance attention. As we can observe in Table 7a, compared against the PVT-like and Swin-like self-attention mechanisms, our CrossFormer outperforms them at least absolute 0.6% accuracy (82.5% vs. 81.9%). The results show that performing the self-attention in a long-short distance manner is most conducive to improving the model's performance.

DPB vs. Other Position Representations. We compare the parameters, FLOPs, throughputs, and accuracies of the models among absolute position embedding (APE), relative position bias (RPB), and DPB. The results are shown in Table 7b. DPB-residual means DPB with residual connections. Both DPB and RPB outperform APE for absolute 0.4% accuracy, which indicates that relative position representations are more beneficial than absolute ones. Further, DPB achieves the same accuracy (82.5%) as RPB with an ignorable extra cost; however, as we described in Section 3.2.2, it is more flexible than RPB and applies to variable image size or group size. The results also show that residual connection in DPB does not help improve or even degrades the model's performance.

5 Conclusions

We proposed a novel transformer-based vision architecture, namely CrossFormer. Its core ingredients are Cross-scale Embedding Layer (CEL) and Long Short Distance Attention (LSDA), thereby yielding the cross-attention module. We further proposed a dynamic position bias, making the relative position bias apply to any input size. Extensive experiments show that CrossFormer achieves superior performance over other state-of-the-art vision transformers on several representative vision tasks. Particularly, CrossFormer is demonstrated to gain great improvements on object detection and segmentation, which indicates that CEL and LSDA are together essential for dense prediction tasks.

REFERENCES

Lei Jimmy Ba, Jamie Ryan Kiros, and Geoffrey E. Hinton. Layer normalization. *CoRR*, abs/1607.06450, 2016.

Tom B. Brown, Benjamin Mann, Nick Ryder, Melanie Subbiah, Jared Kaplan, Prafulla Dhariwal, Arvind Neelakantan, Pranav Shyam, Girish Sastry, Amanda Askell, Sandhini Agarwal, Ariel Herbert-Voss, Gretchen Krueger, Tom Henighan, Rewon Child, Aditya Ramesh, Daniel M. Ziegler, Jeffrey Wu, Clemens Winter, Christopher Hesse, Mark Chen, Eric Sigler, Mateusz Litwin, Scott Gray, Benjamin Chess, Jack Clark, Christopher Berner, Sam McCandlish, Alec Radford, Ilya Sutskever, and Dario Amodei. Language models are few-shot learners. In *Neural Information Processing Systems, NeurIPS*, 2020.

Nicolas Carion, Francisco Massa, Gabriel Synnaeve, Nicolas Usunier, Alexander Kirillov, and Sergey Zagoruyko. End-to-end object detection with transformers. In *Computer Vision - ECCV 2020 - 16th European Conference, Glasgow, UK, August 23-28, 2020, Proceedings, Part I*, volume 12346, pp. 213–229, 2020.

Chun-Fu Chen, Quanfu Fan, and Rameswar Panda. Crossvit: Cross-attention multi-scale vision transformer for image classification. *CoRR*, abs/2103.14899, 2021a.

Chun-Fu Chen, Rameswar Panda, and Quanfu Fan. Regionvit: Regional-to-local attention for vision transformers. *CoRR*, abs/2106.02689, 2021b.

Kai Chen, Jiaqi Wang, Jiangmiao Pang, Yuhang Cao, Yu Xiong, Xiaoxiao Li, Shuyang Sun, Wansen Feng, Ziwei Liu, Jiarui Xu, Zheng Zhang, Dazhi Cheng, Chenchen Zhu, Tianheng Cheng, Qijie Zhao, Buyu Li, Xin Lu, Rui Zhu, Yue Wu, Jifeng Dai, Jingdong Wang, Jianping Shi, Wanli Ouyang, Chen Change Loy, and Dahua Lin. MMDetection: Open mmlab detection toolbox and benchmark. *arXiv preprint arXiv:1906.07155*, 2019.

Xiangxiang Chu, Zhi Tian, Yuqing Wang, Bo Zhang, Haibing Ren, Xiaolin Wei, Huaxia Xia, and Chunhua Shen. Twins: Revisiting spatial attention design in vision transformers. *CoRR*, abs/2104.13840, 2021.

MMSegmentation Contributors. MMSegmentation: Openmmlab semantic segmentation toolbox and benchmark, 2020.

Ekin Dogus Cubuk, Barret Zoph, Jon Shlens, and Quoc Le. Randaugment: Practical automated data augmentation with a reduced search space. In *Neural Information Processing Systems, NeurIPS*, 2020.

Jacob Devlin, Ming-Wei Chang, Kenton Lee, and Kristina Toutanova. BERT: pre-training of deep bidirectional transformers for language understanding. In *Conference of the North American Chapter of the Association for Computational Linguistics, NAACL*, pp. 4171–4186, 2019.

Alexey Dosovitskiy, Lucas Beyer, Alexander Kolesnikov, Dirk Weissenborn, Xiaohua Zhai, Thomas Unterthiner, Mostafa Dehghani, Matthias Minderer, Georg Heigold, Sylvain Gelly, Jakob Uszkoreit, and Neil Houlsby. An image is worth 16x16 words: Transformers for image recognition at scale. In *International Conference on Learning Representations, ICLR*, 2021.

Kai Han, An Xiao, Enhua Wu, Jianyuan Guo, Chunjing Xu, and Yunhe Wang. Transformer in transformer. *CoRR*, abs/2103.00112, 2021.

Kaiming He, Georgia Gkioxari, Piotr Dollár, and Ross B. Girshick. Mask R-CNN. In *International Conference on Computer Vision, ICCV*, pp. 2980–2988, 2017.

Gao Huang, Yu Sun, Zhuang Liu, Daniel Sedra, and Kilian Q. Weinberger. Deep networks with stochastic depth. In Bastian Leibe, Jiri Matas, Nicu Sebe, and Max Welling (eds.), *European Conference on Computer Vision, ECCV*, volume 9908, pp. 646–661, 2016.

Zilong Huang, Youcheng Ben, Guozhong Luo, Pei Cheng, Gang Yu, and Bin Fu. Shuffle transformer: Rethinking spatial shuffle for vision transformer. *CoRR*, abs/2106.03650, 2021.

Diederik P. Kingma and Jimmy Ba. Adam: A method for stochastic optimization. In *International Conference on Learning Representations, ICLR*, 2015.

Alexander Kirillov, Ross B. Girshick, Kaiming He, and Piotr Dollár. Panoptic feature pyramid networks. In *Conference on Computer Vision and Pattern Recognition, CVPR*, pp. 6399–6408, 2019.

Hezheng Lin, Xing Cheng, Xiangyu Wu, Fan Yang, Dong Shen, Zhongyuan Wang, Qing Song, and Wei Yuan. CAT: cross attention in vision transformer. *CoRR*, abs/2106.05786, 2021.

Tsung-Yi Lin, Michael Maire, Serge J. Belongie, James Hays, Pietro Perona, Deva Ramanan, Piotr Dollár, and C. Lawrence Zitnick. Microsoft COCO: common objects in context. In *European Conference on Computer Vision, ECCV*, volume 8693, pp. 740–755, 2014.

Tsung-Yi Lin, Priya Goyal, Ross B. Girshick, Kaiming He, and Piotr Dollár. Focal loss for dense object detection. *Transactions on Pattern Analysis and Machine Intelligence, PAMI*, 42(2):318–327, 2020.

Yun Liu, Guolei Sun, Yu Qiu, Le Zhang, Ajad Chhatkuli, and Luc Van Gool. Transformer in convolutional neural networks. *CoRR*, abs/2106.03180, 2021a.

Ze Liu, Yutong Lin, Yue Cao, Han Hu, Yixuan Wei, Zheng Zhang, Stephen Lin, and Baining Guo. Swin transformer: Hierarchical vision transformer using shifted windows. *CoRR*, abs/2103.14030, 2021b.

Vinod Nair and Geoffrey E. Hinton. Rectified linear units improve restricted boltzmann machines. In Johannes Fürnkranz and Thorsten Joachims (eds.), *International Conference on Machine Learning, ICML*, pp. 807–814, 2010.

Zizheng Pan, Bohan Zhuang, Jing Liu, Haoyu He, and Jianfei Cai. Scalable visual transformers with hierarchical pooling. *CoRR*, abs/2103.10619, 2021.

Olga Russakovsky, Jia Deng, Hao Su, Jonathan Krause, Sanjeev Satheesh, Sean Ma, Zhiheng Huang, Andrej Karpathy, Aditya Khosla, Michael S. Bernstein, Alexander C. Berg, and Fei-Fei Li. Imagenet large scale visual recognition challenge. *International Journal of Computer Vision, IJCV*, 2015.

Peter Shaw, Jakob Uszkoreit, and Ashish Vaswani. Self-attention with relative position representations. In *Conference of the North American Chapter of the Association for Computational Linguistics: Human Language Technologies, NAACL*, pp. 464–468, 2018.

Aravind Srinivas, Tsung-Yi Lin, Niki Parmar, Jonathon Shlens, Pieter Abbeel, and Ashish Vaswani. Bottleneck transformers for visual recognition. In *Conference on Computer Vision and Pattern Recognition, CVPR*, 2021.

Hugo Touvron, Matthieu Cord, Matthijs Douze, Francisco Massa, Alexandre Sablayrolles, and Hervé Jégou. Training data-efficient image transformers & distillation through attention. In *International Conference on Machine Learning, ICML*, volume 139, pp. 10347–10357, 2021.

Ashish Vaswani, Noam Shazeer, Niki Parmar, Jakob Uszkoreit, Llion Jones, Aidan N. Gomez, Lukasz Kaiser, and Illia Polosukhin. Attention is all you need. In *Neural Information Processing Systems, NeurIPS*, pp. 5998–6008, 2017.

Wenhai Wang, Enze Xie, Xiang Li, Deng-Ping Fan, Kaitao Song, Ding Liang, Tong Lu, Ping Luo, and Ling Shao. Pyramid vision transformer: A versatile backbone for dense prediction without convolutions. *CoRR*, abs/2102.12122, 2021.

Haiping Wu, Bin Xiao, Noel Codella, Mengchen Liu, Xiyang Dai, Lu Yuan, and Lei Zhang. Cvt: Introducing convolutions to vision transformers. *CoRR*, abs/2103.15808, 2021.

Tete Xiao, Yingcheng Liu, Bolei Zhou, Yuning Jiang, and Jian Sun. Unified perceptual parsing for scene understanding. In *European Conference on Computer Vision, ECCV*, volume 11209, pp. 432–448, 2018.

Yufei Xu, Qiming Zhang, Jing Zhang, and Dacheng Tao. Vitae: Vision transformer advanced by exploring intrinsic inductive bias. *CoRR*, abs/2106.03348, 2021.

Li Yuan, Yunpeng Chen, Tao Wang, Weihao Yu, Yujun Shi, Francis E. H. Tay, Jiashi Feng, and Shuicheng Yan. Tokens-to-token vit: Training vision transformers from scratch on imagenet. *CoRR*, abs/2101.11986, 2021.

Sangdoo Yun, Dongyoon Han, Sanghyuk Chun, Seong Joon Oh, Youngjoon Yoo, and Junsuk Choe. Cutmix: Regularization strategy to train strong classifiers with localizable features. In *International Conference on Computer Vision, ICCV*, pp. 6022–6031, 2019.

Hongyi Zhang, Moustapha Cissé, Yann N. Dauphin, and David Lopez-Paz. mixup: Beyond empirical risk minimization. In *International Conference on Learning Representations, ICLR*, 2018.

Pengchuan Zhang, Xiyang Dai, Jianwei Yang, Bin Xiao, Lu Yuan, Lei Zhang, and Jianfeng Gao. Multi-scale vision longformer: A new vision transformer for high-resolution image encoding. *CoRR*, abs/2103.15358, 2021a.

Qing-Long Zhang and Yubin Yang. Rest: An efficient transformer for visual recognition. *CoRR*, abs/2105.13677, 2021.

Zizhao Zhang, Han Zhang, Long Zhao, Ting Chen, and Tomas Pfister. Aggregating nested transformers. *CoRR*, abs/2105.12723, 2021b.

Zhun Zhong, Liang Zheng, Guoliang Kang, Shaozi Li, and Yi Yang. Random erasing data augmentation. In *Association for the Advancement of Artificial Intelligence, AAAI*, pp. 13001–13008, 2020.

Bolei Zhou, Hang Zhao, Xavier Puig, Sanja Fidler, Adela Barriuso, and Antonio Torralba. Scene parsing through ADE20K dataset. In *Conference on Computer Vision and Pattern Recognition, CVPR*, pp. 5122–5130, 2017.

A CROSSFORMER

A.1 PSEUDO CODE OF LSDA

The pseudo code for LSDA is shown in Algorithm 1. As we can see, based on the vanilla self-attention module, both SDA and LDA are implemented with only ten lines of code, and only *reshape* and *permute* operations are used.

Algorithm 1 LSDA code (PyTorch-like)

```
# H: height, W: width, G: group size of SDA/LDA
# x: input tensor (H, W, D)
class LSDA():
   def forward(x, type):
      ## group the embeddings
      if type == "SDA":
         x = x.reshaspe(H // G, G, W // G, G, D).permute(0, 2, 1, 3, 4)
      elif type == "LDA":
         x = x.reshaspe(G, H // G, G, W // G, D).permute(1, 3, 0, 2, 4)
      x = x.reshape(H * W // (G ** 2), G ** 2, D)

      ## the vanilla self-attention module
      x = Attention(x)

      ## un-group the embeddings
      x = x.reshaspe(H // G, W // G, G, G, D)
      if type == "SDA":
         x = x.permute(0, 2, 1, 3, 4).reshaspe(H, W, D)
      elif type == "LDA":
         x = x.permute(2, 0, 3, 1, 4).reshaspe(H, W, D)
      return x
```

A.2 DYNAMIC POSITION BIAS (DPB)

Figure 4 gives an example of computing $(\Delta x_{ij}, \Delta y_{ij})$ with $G = 5$ in the DPB module. For a group of size $G \times G$, it is easy to deduce that:

$$\begin{aligned} 0 \leq x, y < G \\ 1 - G \leq \Delta x_{ij} \leq G - 1 \\ 1 - G \leq \Delta y_{ij} \leq G - 1. \end{aligned} \tag{3}$$

Thus, motivated by the relative position bias, we construct a matrix $\hat{\boldsymbol{B}} \in \mathbb{R}^{(2G-1)\times(2G-1)}$, where

$$\hat{\boldsymbol{B}}_{i,j} = DPB(1 - G + i, 1 - G + j),\ 0 \leq i, j < 2G - 1. \tag{4}$$

The complexity of computing $\hat{\boldsymbol{B}}$ is $O(G^2)$. Then, the bias matrix $\boldsymbol{B}$ in DPB can be drawn from $\hat{\boldsymbol{B}}$, *i.e.*,

$$\boldsymbol{B}_{i,j} = \hat{\boldsymbol{B}}_{\Delta x_{ij}, \Delta y_{ij}}. \tag{5}$$

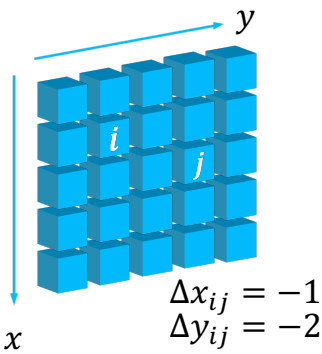

Figure 4: An example of computing $(\Delta x_{ij}, \Delta y_{ij})$.

When the image/group size (*i.e.*, G) is fixed, both $\hat{\boldsymbol{B}}$ and $\boldsymbol{B}$ will be also unchanged in the test phase. Therefore, we only need to compute $\hat{\boldsymbol{B}}$ and $\boldsymbol{B}$ once, and DPB is equivalent to relative position bias in this case.

A.3 VARIANTS OF CROSSFORMER FOR DETECTION AND SEGMENTATION

We test two different backbones for dense prediction tasks. The variants of CrossFormer for dense prediction (object detection, instance segmentation, and semantic segmentation) are in Table 8. The architectures are the same as those for image classification except that different G and I in the first two stages are used. Notably, group size (*i.e.*, G and I) does not affect the shape of weight tensors, so backbones pre-trained on ImageNet can be fine-tuned directly on other tasks even if they use different G and I.

Table 8: CrossFormer-based backbones for object detection and semantic/instance segmentation. The example input size is 1280×800. D and H mean embedding dimension and the number of heads in the multi-head self-attention module, respectively. G and I are group size and interval for SDA and LDA, respectively.

	Output Size	Layer Name	CrossFormer-T	CrossFormer-S	CrossFormer-B	CrossFormer-L
Stage-1	320×200	Cross Embed.	Kernel size: 4×4, 8×8, 16×16, 32×32, Stride=4			
		SDA/LDA MLP	$\begin{bmatrix} D_1 = 64 \\ H_1 = 2 \\ G_1 = 14 \\ I_1 = 16 \end{bmatrix} \times 1$	$\begin{bmatrix} D_1 = 96 \\ H_1 = 3 \\ G_1 = 14 \\ I_1 = 16 \end{bmatrix} \times 2$	$\begin{bmatrix} D_1 = 96 \\ H_1 = 3 \\ G_1 = 14 \\ I_1 = 16, \end{bmatrix} \times 2$	$\begin{bmatrix} D_1 = 128 \\ H_1 = 4 \\ G_1 = 14 \\ I_1 = 16 \end{bmatrix} \times 2$
Stage-2	160×100	Cross Embed.	Kernel size: 2×2, 4×4, Stride=2			
		SDA/LDA MLP	$\begin{bmatrix} D_2 = 128 \\ H_2 = 4 \\ G_2 = 14 \\ I_2 = 8 \end{bmatrix} \times 1$	$\begin{bmatrix} D_2 = 192 \\ H_2 = 6 \\ G_2 = 14 \\ I_2 = 8 \end{bmatrix} \times 2$	$\begin{bmatrix} D_2 = 192 \\ H_2 = 6 \\ G_2 = 14 \\ I_2 = 8 \end{bmatrix} \times 2$	$\begin{bmatrix} D_2 = 256 \\ H_2 = 8 \\ G_2 = 14 \\ I_2 = 8 \end{bmatrix} \times 2$
Stage-3	80×50	Cross Embed.	Kernel size: 2×2, 4×4, Stride=2			
		SDA/LDA MLP	$\begin{bmatrix} D_3 = 256 \\ H_3 = 8 \\ G_3 = 7 \\ I_3 = 2 \end{bmatrix} \times 8$	$\begin{bmatrix} D_3 = 384 \\ H_3 = 12 \\ G_3 = 7 \\ I_3 = 2 \end{bmatrix} \times 6$	$\begin{bmatrix} D_3 = 384 \\ H_3 = 12 \\ G_3 = 7 \\ I_3 = 2 \end{bmatrix} \times 18$	$\begin{bmatrix} D_3 = 512 \\ H_3 = 16 \\ G_3 = 7 \\ I_3 = 2 \end{bmatrix} \times 18$
Stage-4	40×25	Cross Embed.	Kernel size: 2×2, 4×4, Stride=2			
		SDA/LDA MLP	$\begin{bmatrix} D_4 = 512 \\ H_4 = 16 \\ G_4 = 7 \\ I_4 = 1 \end{bmatrix} \times 6$	$\begin{bmatrix} D_4 = 768 \\ H_4 = 24 \\ G_4 = 7 \\ I_4 = 1 \end{bmatrix} \times 2$	$\begin{bmatrix} D_4 = 768 \\ H_4 = 24 \\ G_4 = 7 \\ I_4 = 1 \end{bmatrix} \times 2$	$\begin{bmatrix} D_4 = 1024 \\ H_4 = 32 \\ G_4 = 7 \\ I_4 = 1 \end{bmatrix} \times 2$

Table 9: Object detection results on COCO *val* 2017. "Memory" means the allocated memory per GPU reported by $torch.cuda.max_memory_allocated()$. ‡ indicates that models use different (G, I) from classification models.

Method	Backbone	G_1	I_1	G_2	I_2	Memory	#Params	FLOPs	AP^b	AP^b_{50}	AP^b_{75}
RetinaNet 1× schedule	CrossFormer-S	7	8	7	4	14.7G	40.8M	282.0G	44.4	65.8	47.4
	CrossFormer-S‡	14	16	14	8	11.9G	40.8M	272.1G	44.2	65.7	47.2
	CrossFormer-B	7	8	7	4	22.8G	62.1M	389.0G	46.2	67.8	49.5
	CrossFormer-B‡	14	16	14	8	20.2G	62.1M	379.0G	46.1	67.7	49.0
Mask-RCNN 1× schedule	CrossFormer-S	7	8	7	4	15.5G	50.2M	301.0G	45.4	68.0	49.7
	CrossFormer-S‡	14	16	14	8	12.7G	50.2M	291.1G	45.0	67.9	49.1
	CrossFormer-B	7	8	7	4	23.8G	71.5M	407.9G	47.2	69.9	51.8
	CrossFormer-B‡	14	16	14	8	21.0G	71.5M	398.1G	47.1	69.9	52.0

Table 10: Semantic segmentation results on ADE20K validation set with semantic FPN or UPerNet as heads.

Backbone	G_1	I_1	G_2	I_2	Semantic FPN (80K iterations)				UPerNet (160K iterations)				
					Memory	#Params	FLOPs	IOU	Memory	#Params	FLOP	IOU	MS IOU
CrossFormer-S	7	8	7	4	20.9G	34.3M	220.7G	46.0	–	62.3M	979.5G	47.6	48.4
CrossFormer-S‡	14	16	14	8	20.9G	34.3M	209.8G	46.4	14.6G	62.3M	968.5G	47.4	48.2
CrossFormer-B	7	8	7	4	14.6G	55.6M	331.0G	47.7	15.8G	83.6M	1089.7G	49.7	50.6
CrossFormer-B‡	14	16	14	8	14.6G	55.6M	320.1G	48.0	15.8G	83.6M	1078.8G	49.2	50.1
CrossFormer-L	7	8	7	4	25.3G	95.4M	497.0G	48.7	18.1G	125.5M	1257.8G	50.4	51.4
CrossFormer-L‡	14	16	14	8	25.3G	95.4M	482.7G	49.1	18.1G	125.5M	1243.5G	50.5	51.4

B EXPERIMENTS

B.1 OBJECT DETECTION

Table 9 provides more results on object detection with RetinaNet and Mask-RCNN as detection heads. As we can see, a smaller (G, I) achieves a higher AP than a larger one, but the performance gain is marginal. Considering that a larger (G, I) can save more memory cost, we think $(G_1 = 14, I_1 = 16, G_2 = 14, I_2 = 8)$, which accords with configurations in Table 8, achieves a better trade-off between the performance and cost.

B.2 SEMANTIC SEGMENTATION

Similar to object detection, we test two different configurations of (G, I) for semantic segmentation's backbones. The results are shown in Table 10. As we can see, the memory costs of the two configurations are almost the same, which is different from experiments on object detection. Further, when taking semantic FPN as the detection head, CrossFormers‡ show advantages over CrossFormers on both IOU (*e.g.*, 46.4 vs. 46.0) and FLOPs (*e.g.*, 209.8G vs. 220.7G). When taking UPerNet as the segmentation head, a smaller (G, I) achieves higher performance like object detection.